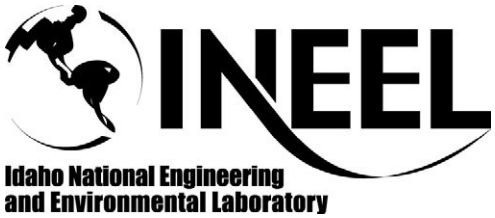

INEEL/CON-05-02578
PREPRINT

Localized Corrosion Of A Neutron Absorbing Ni-Cr-Mo-Gd Alloy

R. E. Mizia
T. E. Lister
P. J. Pinhero
T L. Trowbridge

April 3-7, 2005

CORROSION 2005

LOCALIZED CORROSION OF A NEUTRON ABSORBING Ni-Cr-Mo-Gd ALLOY

R. E. Mizia, T. E. Lister, P. J. Pinhero, T. L. Trowbridge
Idaho National Laboratory
P.O. Box 1625
Idaho Falls, ID 83415, USA

ABSTRACT

The National Spent Nuclear Fuel Program, located at the Idaho National Laboratory (INL), has developed a new nickel-chromium-molybdenum-gadolinium structural alloy for storage and long-term disposal of spent nuclear fuel (SNF). The new alloy will be used for SNF storage container inserts for nuclear criticality control. Gadolinium has been chosen as the neutron absorption alloying element due to its high thermal neutron absorption cross section. This alloy must be resistant to localized corrosion when exposed to postulated Yucca Mountain in-package chemistries. The corrosion resistance properties of three experimental heats of this alloy are presented. The alloys performance are be compared to Alloy 22 and borated stainless steel. The results show that initially the new Ni-Cr-Mo-Gd alloy is less resistant to corrosion as compared to another Ni-Cr-Mo-Gd alloy (Alloy 22); but when the secondary phase that contains gadolinium (gadolinide) is dissolved, the alloy surface becomes passive.

The focus of this work is to qualify these gadolinium containing materials for ASME code qualification and acceptance in the Yucca Mountain Repository.

Keywords: neutron absorbing material, nickel-based alloy, gadolinium, Yucca Mountain, corrosion rate, localized corrosion

INTRODUCTION

The U.S. Department of Energy (DOE) is tasked with the management and disposal of DOE-owned spent nuclear fuel (SNF). The SNF management approach is to package SNF in the DOE standard canister that will hold it during interim storage, transportation, and final disposal at the Yucca Mountain Repository. The standard canister will need a corrosion-resistant alloy for neutron-absorbing structural inserts for criticality control because of the fuel enrichment and total quantity of fissile material in some DOE SNF. These structural inserts will also provide SNF geometry control. The

structural inserts and the DOE standard canister are shown in Figure 1. This alloy must be corrosion resistant under the projected storage conditions so as not to leach out the neutron-absorbing element (neutron poison). The time of greatest significance is when the repository aqueous environment reaches the inside of the canister after a postulated breach of the outer waste package barriers. Other technical requirements are that this alloy be weldable, have acceptable mechanical properties for American Society of Mechanical Engineers (ASME) code approval, and be produced using conventional ingot metallurgy techniques.

The initial alloy development work focused on 316L stainless steel alloyed with gadolinium. The use of another neutron absorbing structural material, boron-containing stainless steel, was ruled out because of boron's lower thermal neutron absorption properties as compared to gadolinium. The microstructure, mechanical properties, and corrosion resistance of these alloys have been described elsewhere.[1,2,3] These studies were unable to measure gadolinium in the austenitic matrix of the 316L stainless. The gadolinium solidifies as a second phase. The study of 316L-based alloys was discontinued due to hot workability problems (low hot ductility) associated with the low liquation temperature and extended melting temperature range of this $(Fe,Ni,Cr)_3Gd$ secondary, intermetallic phase. With these 316L-based alloys, the hot workability range was restricted to a narrow temperature range around 950°C.

The alloy development program shifted to using the Ni-Cr-Mo alloy system. The Alloy 22 (UNS N06022) material that is specified for the Yucca Mountain Waste Package Outer Barrier is an alloy of this type. The resulting microstructure, mechanical properties, and results of initial corrosion testing have been described earlier.[4,5] These alloys solidify with the formation of a primary austenite matrix and a terminal, eutectic-like secondary phase constituent as shown in Figure 2. The composition of this second phase was measured with Electron Microprobe Analysis (EPMA) and electron backscattered diffraction (EBSD). EBSD analysis identified the second phase as a $(Ni,Cr)_5Gd$ intermetallic mixed with other dissolved elements such as molybdenum and iron. This gadolinium-rich phase is referred to as a gadolinide. As with the stainless alloys, this intermetallic phase will affect the mechanical properties and the corrosion resistance of these Ni-Cr-Mo-Gd alloys.

This new material is now covered under American Society of Testing and Materials (ASTM) B932-04[6] (UNS N06464) with the chemistry requirements shown in Table 1. An ASME Code Case Inquiry was submitted to approve the material for Section III, Division 3 applications.[7]

EXPERIMENTAL PROCEDURE

Ingot/Plate Preparation

The heat chemistries for the Ni-Cr-Mo-Gd alloys are shown in Table 2. Heat M322 was produced by Vacuum Induction Melting (VIM) with a 300-lb initial melt that was vacuum cast into two 10-cm (3.9-in.) diameter equal length round bars. These bars were Vacuum Arc Remelted (VAR) under approximately 130 Pa (1 torr) of helium pressure into a 14.3-cm diameter ingots weighing approximately 64 kg (140 lb). M322 has a higher gadolinium level than allowed by the ASTM B 932 because it was prepared early in the development program where a target level of 2.25 to 2.5 wt% gadolinium was being studied for better neutronic performance. M326 and M327 were smaller VIM/VAR ingots with a finished size before rolling of 5 in. diameter by 8.5 in. long. Heat M326 meets the chemistry requirements of ASTM B932. M327 was formulated to study the effect of a higher chromium level on performance. All ingots were hot rolled to a plate with the approximate dimensions of 1.5 cm (0.6 in.) thick by 15 cm (6 in.) wide. The ingots were homogenized at 1160°C (2125°F) +/- 14°C (25°F) for 16 hours prior to rolling, and then reheated between rolling passes as necessary. Following rolling, the plate was solution annealed at 1160°C (2125°F) +/- 14°C (25°F) for 4 hours and water quenched.

Comparisons were also made with Alloy 22 and a borated stainless steel, whose chemistries are shown in Table 3.

Electrochemical Corrosion Testing

Corrosion properties of the Ni-Cr-Mo-Gd alloy heats were evaluated using two electrochemical methods: cyclic potentiodynamic polarization (CPP) and potentiostatic (PS) polarization. The following electrolytes were used: (a) 0.1 M HCl, 30°C and (b) 0.028 M NaCl, 30°C. The acidic chloride was chosen for known localized corrosion initiation and is a bounding case for early waste package failure.

Cylindrical specimens (6.3 mm by 42 mm long) were machined from plate of approximately 15 mm thickness. The specimens were degreased by sonication in acetone followed by ethanol. An initial mass was measured. The clean, mounted specimen was placed into a freshly purged corrosion cell, as specified by ASTM G5,[8] fitted with two graphite rod auxiliary electrodes, a saturated calomel electrode (SCE) reference connected through a luggin capillary, and a gas purge. The cell contained 1 L of test solution. The entire assembly was thermostatically maintained in a water bath.

The CPP test follows the requirements of ASTM G 61.[9] The corrosion potential was first measured for 50 minutes prior to the CPP scan. CPP scans were then acquired from the equilibrated corrosion potential to +1.0 V vs. SCE. The potential sweep rate was 0.6 V/hour. PS testing of a duplicate specimen, prepared in the same manner as the CPP tests, was performed at 0.20 V vs. SCE in all solutions up to 50 hours. The value of 0.20 V was selected because it is the lowest potential where pronounced corrosion activity occurs in Cl^--containing media.[4,5] and is believed that this potential corresponds to dissolution of the surface-exposed gadolinide phase.

Long Term Immersion Testing

In addition to electrochemical testing, two long-term exposure tests have been performed in Yucca Mountain Project solutions J-13 and J-13 50X[10,11] (Table 4). The J-13 solution is considered to be representative of the in-drift seepage water chemistry. The 50X J-13 solution multiplies the ionic content of J-13 fifty times. The testing procedure, which is based on ASTM G31[12] involves exposing triplicate M322 specimens (4.1 × 1.3 × 0.4 cm) to the solutions at 30°C (86°F) with gravimetric analysis performed at selected intervals. The specimen weight loss and the calculated surface area were used to calculate the general corrosion rate. A descaling procedure from ASTM G 1[13] was used to clean the specimens exposed to both the J-13 and J-13 50X solutions.

Scanning Electron Microscopy

Following corrosion testing, the microstructural changes were documented with scanning electron microscopy (SEM). Both secondary electron (SE) and backscattered electron (BSE) imaging provide information about the topography and secondary phases, respectively. In addition to imaging, energy dispersive spectra (EDS) were also acquired to provide information about the chemistry of each phase. Dual beam Focused Ion Beam (FIB) SEM, courtesy of Sandia National Laboratory, was also used to cross section through secondary phases and corroded areas. SEM of FIB cross-sectioned specimens was completed at the INL.

RESULTS

Electrochemical Corrosion Test Results

Part 1: Ni-Cr-Mo-Gd alloy corrosion performance. Figure 3 shows CPP scans for specimens of M327 and Alloy 22 in 0.1 M HCl at 30ºC (86°F). The M327 specimen displays a large rise in current starting from the corrosion potential, which has been attributed to the dissolution of the secondary gadolinide phase.[4,5] Following a peak at -0.2 V, the current declines until the transpassive region (about 0.8 V). The reverse scan has a lower current over most of the passive region. Although not shown here, a second CPP scan of the same specimen results in a much lower current due, attributed to the removal of most of the exposed gadolinide particles from the surface from the first scan. SEM analysis following CPP testing has shown that the gadolinide particles have been dissolved to the point where none were found by SEM backscatter imaging. The surfaces were roughened by the 2−10 μm diameter pits where the particles resided.[4,5] The Alloy 22 specimen does not show any indication of localized attack due to the passive nature of the material and lack of a secondary phase.

Figure 4 compares the performance of alloys M326 and M327 in 0.028 M NaCl at 30°C (86ºF). The M327 alloy has a higher chromium level as compared to M326 (Table 2). The additional chromium was added to study its effect on passivity. Figure 4A shows that in the CPP test the current density seems to be controlled by dissolution of the gadolinide phase. The extra chromium content does not have a measurable effect on the passive current. However, in the PS test (Figure 4B) at 0.2 V, the current density of the M327 specimen is much lower than the M326 specimen, which shows the beneficial effect of the additional chromium in M327.

Part 2: Ni-Cr-Mo-Gd vs 304B6 SS. Figure 5 shows CPP scans for M327 and 304B6 specimens in 0.028 M NaCl as a comparison of the corrosion properties of the two materials. The M327 specimen again shows a large rise in current starting from the corrosion potential and peaking at 0.2 V in a manner much like that described above for tests in 0.1 M HCl. Hysteresis is not observed in this case, suggesting that the base material is stable in the passive region. The 304B6 specimen does not show significant current in the forward scan until about 0.25 V, where the initiation of breakdown occurs. There is a significant hysteresis current flow on the reverse scan with the sample not reaching a repassivation state at the original corrosion potential value (-0.029 V) where the scan ends. This suggests that the material may not be stable to localized corrosion in this solution. Recently published results on the corrosion performance of borated stainless steel suggests that these alloys are susceptible to localized corrosion at or near the secondary boride phase when exposed to an acidic, chloride containing solution.[14,15]

Damage to the M327 specimen observed following the CPP is much like that observed in 0.1 M HCl as documented in previous work[4,5] and as discussed above. The 304B6 suffered far worse damage from the test. SEM images of the specimen examined in Figure 5 are shown in Figure 6. The type of pitting shown in Figure 6 was observed throughout the specimen. The damage appears to be much more extensive as the bottom of the pits could not be observed with SEM or LOM. FIB milling revealed that the pits have extensive undercutting as shown in Figure 7. Following removal of an area around a small pit, the entire exposed area was a skin of material with open region below where a large cavity apparently has been formed. This type of phenomenon of extensive damage was also observed for the 304B6 specimen in the tests below.

Figure 8 shows PS curves obtained by poising M327 and 304B6 specimens at 0.2 V at 60°C (140°F) in 0.1 M HCl. The 304B6 specimen shows almost four orders of magnitude higher current during the test and resulted in extensive damage to the surface as shown in Figure 9. The 304B6 specimen lost 32% of its mass and displayed extensive “sugaring” (particles chunking out of the sample

following the test). The potentiostat could not deliver enough current to maintain the potential at 0.2 V for the 304B6 specimen, possibly the reason a relatively flat response curve was observed. The M327 specimen shows a high current initially, then quickly drops to below 1 $\mu A/cm^2$, where a corrosion rate based on current of 4.2 μm/yr was calculated at the final current point using ASTM G102 procedures.[16] The photograph of the M327 specimen in Figure 9 reveals very little change in the appearance. Light Optical Microscopy (LOM) imaging (not shown) indicates that the gadolinide phase was removed from the specimen during the test.

Long Term Immersion Test Results

Ni-Cr-Mo-Gd alloys were immersed in J-13 and J-13 50X solutions at 30°C (86°F) for long periods with intermittent examination. Figure 10 shows a plot of the corrosion rate derived from the weight loss during the tests using the ASTM G31-72[13] immersion method. The corrosion rates for specimens exposed to J-13 rapidly decrease to values below 100 nm/yr with the final value of 8.3 nm/yr obtained at just under 2 years exposure. The J-13 50X specimen exhibited higher corrosion rates, as would be expected due to the higher ionic concentration. Note that early tests used a cleaning method that did not adequately remove scale for J-13 50X specimens and thus early corrosion rates for those specimens are not shown. The immersion tests were terminated at the last data point in Figure 10 and further microstructural analysis was performed as described below.

Images taken of the immersion specimens after the total exposure time are shown in Figures 11 and 12. The LOM images of the J-13 exposed sample (Figure 11) indicate staining and light pitting isolated at the gadolinide particles while the high resolution SEM image (Figure 12) shows the initiation of microscopic pitting on the gadolinide particles. The J-13 50X sample shows more extensive loss of the gadolinide particles in both LOM and SEM images. The SEM image of the J-13 50X sample (Figure 12) shows a partially dissolved gadolinide particle (see arrow designating particle) where microscopic pitting is evident. Most of the gadolinide particles were totally dissolved by the nearly 2-year exposure to J-13 50X solution. No evidence of attack of the base material was observed in the analysis, suggesting that the base material is resistant to localized attack under these conditions and may protect the remainder of the surface from further degradation. This also points to the use of the corrosion rate in work, as this is a general corrosion description, and the attack here is localized in nature. It does, however, provide a useful number to describe the amount of damage.

CONCLUSIONS AND SUMMARY

The corrosion resistance of these Ni-Cr-Mo-Gd alloys is dependent on the amount of gadolinium addition, which will determine the amount of the gadolinide that will be present in the alloy matrix. The gadolinide that intersects the surface exposed to acidic aqueous solutions and other solutions simulating the Yucca Mountain environment might be preferentially attacked and removed, but the underlying Ni-Cr-Mo matrix will then repassivate, and the corrosion rate will drop off to an extremely low rate. The borated Type 304B6 stainless steel was found to be susceptible to localized corrosion in electrochemical tests.

ACKNOWLEDGEMENTS

This work was supported by the U.S. Department of Energy, Assistant Secretary for Environmental Management, under DOE Idaho Operations Office Contract No. DE-AC07-99ID13727. This work was performed at the Idaho National Laboratory, formerly Idaho National Engineering and Environmental Laboratory (INEEL) through support from the National Spent Nuclear Fuel Program.

REFERENCES

[1] *Development of Gadolinium-Containing Stainless Steels,* DOE/SNF/REP-066, Idaho National Engineering and Environmental Laboratory, January 2001.

[2] R. E. Mizia, P. J. Pinhero, T. E. Lister, J. N. DuPont and C. V. Robino, "Corrosion Performance of a Gadolinium-Containing Stainless Steel," Paper 138, Corrosion 2001, NACE International, Houston, Texas.

[3] J. N. Dupont, C. V. Robino, and R. E. Mizia, "Development of Gadolinium Containing Stainless Steels for Nuclear Criticality Control," TMS 2000 Fall Meeting, TMS Society, St. Louis, Missouri.

[4] R. E. Mizia, T. E. Lister, P. J. Pinhero, C. V. Robino, and J. N. DuPont,"Microstructure and Corrosion Performance of a Neutron Absorbing Ni-Cr-Mo-Gd Alloy," Paper # 03679, Corrosion 2003, NACE International, Houston, Texas.

[5] *Interim Report on the Corrosion Performance of a Neutron Absorbing Ni-Cr-Mo-Gd Alloy,* DOE/SNF/REP-086, Idaho National Engineering and Environmental Laboratory, March 2004.

[6] ASTM B932-04, *Standard Specification for Low-Carbon Nickel-Chromium-Molybdenum-Gadolinium Alloy Plate, Sheet, and Strip*, American Society for Testing and Materials, West Conshohocken, Pennsylvania, 2004.

[7] ASME Boiler and Pressure Vessel Code, Section III, Division 3, *Containment Systems and Transport Packagings for Spent Nuclear Fuel and High-Level Radioactive Waste,* The American Society of Mechanical Engineers, New York, New York, 2002.

[8] ASTM G5-94, *Standard Reference Test Method for Making Potentiostatic and Potentiodynamic Anodic Polarization Measurements,* American Society for Testing and Materials, West Conshohocken, Pennsylvania, 2002.

[9] ASTM G 61-86, *Standard Test Method for Conducting Cyclic PotentiodynamicPolarization Measurements for Localized Corrosion Susceptibility of Iron-, Nickel-, or Cobalt- Based Alloys*, American Society for Testing and Materials, West Conshohocken, Pennsylvania, 2002.

[10] J. Harrar, J. Carley, W. Isherwood, and E. Raber, "Report of the Committee to Review the Use of J-13 Well Water in Nevada Nuclear Waste Storage Investigation," UCID-21867, Lawrence Livermore National Laboratory, January 1990.

[11] *In-Package Chemistry for Waste Forms, ANL-EBS-MD-000056, REV00,* US DOE Office of Civilian Radioactive Waste Management, March 15, 2001.

[12] ASTM G31-72 (Reapproved 1999), *Standard Practice for Laboratory Immersion Corrosion Testing of Metals*, ASTM, West Conshohocken, Pennsylvania, 1999.

[13] ASTM G1-03, *Standard Practice for Preparing, Cleaning, and Evaluating Corrosion Test Specimens,* American Society for Testing and Materials, West Conshohocken, Pennsylvania, 2003.

[14] D. A. Moreno, B. Molina, C. Ranniger, F. Montero, and J. Izquierdo, "Microstructural Characterization and Pitting Corrosion Behavior of UNS S30466 Borated Stainless Steel," Corrosion-Vol. 60, No. 6, pages 573–583, NACE International, Houston, Texas, 2004.

[15] D. V. Fix, J. C. Estill, L. Wong, and R. B. Rebak, "General and Localized Corrosion of Austenitic and Borated Stainless Steels in Simulated Concentrated Ground Waters," pages 127–149, PVP2004-2792, The 2004 ASME/JSME Pressure Vessels and Piping Conference, The American Society of Mechanical Engineers, New York, New York, 2004.

[16] ASTM G102-89 (reapproved 1999), *Standard Practice for Calculation of Corrosion Rates and Related Information from Electrochemical Measurements*, American Society for Testing and Materials, West Conshohocken, Pennsylvania, 1999.

TABLE 1
CHEMICAL REQUIREMENTS PER ASTM B932-04[6]

Composition Limits (wt%)	
Element	Alloy N06464
Molybdenum	13.1 to 16.0
Chromium	14.5 to 17.1
Iron	1.0 max
Cobalt, max	2.0
Carbon, max	0.010
Silicon, max	0.08
Manganese, max	0.5
Phosphorus, max	0.005
Sulfur, max	0.005
Nickel	Remainder[a]
Oxygen	0.005
Nitrogen, max	0.010
Gadolinium	1.9 to 2.1
a. Shall be determined arithmetically by difference.	

TABLE 2
CHEMICAL ANALYSIS OF HEATS M322, M326, M327

Element	M322 (VIM/VAR)	M326 (VIM/VAR)	M327 (VIM/VAR)
Mo	14.71	14.53	14.32
Cr	14.93	14.71	21.01
Gd	2.38	2.00	1.98
O	0.0022	0.0032	0.0042
Mn	<0.001	<0.001	<0.01
Mg	<0.001	0.002	0.002
Ni	Bal	Bal	Bal
Fe	0.028	0.025	0.0032
Co	<0.001	0.009	0.003
C	<0.01	0.006	<0.001
Si	<0.01	0.013	0.018
S	<0.0002	<0.001	0.002
Ti	<0.005	—	—
Al	0.005	—	—

TABLE 3
CHEMICAL ANALYSIS FOR ALLOY 22 AND BORATED STAINLESS STEEL

Element	UNS N06022 Heat 2277-7-3130	Type 304B6, Grade A Heat 182196
C	0.003	0.05
Co	0.74	NR
Cr	21.55	18.93
Fe	3.54	Balance
B	—	1.70
Mn	0.25	1.68
Mo	13.47	NR
N	NR	0.005
Ni	Balance	13.15
P	0.07	0.005
S	0.004	0.003
Si	0.024	0.57
W	2.83	—

TABLE 4
COMPOSITION OF YUCCA MOUNTAIN PROJECT CORROSION SOLUTIONS

	Concentration (mg/L)	
Ion	J-13 Well Water	50X J-13
K	5.04	252
Na	45.8	2,290
Mg	2.01	101
Ca	13.0	650
F	2.18	109
Cl	7.14	357
NO_3	8.78	439
SO_4	18.4	920
HCO_3	128.9	6,455
Si (aq)	28.5	1,425
pH	7.14	—

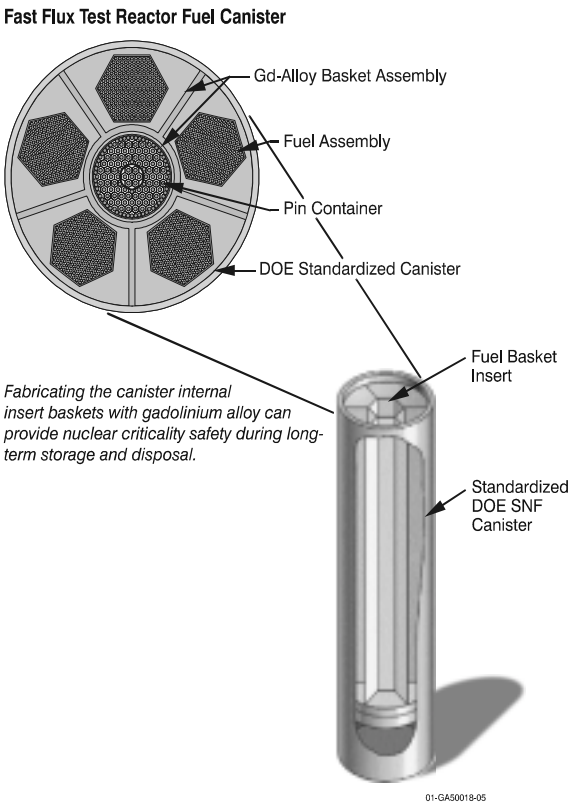

FIGURE 1 - DOE Standard Canister with neutron absorbing structural insert

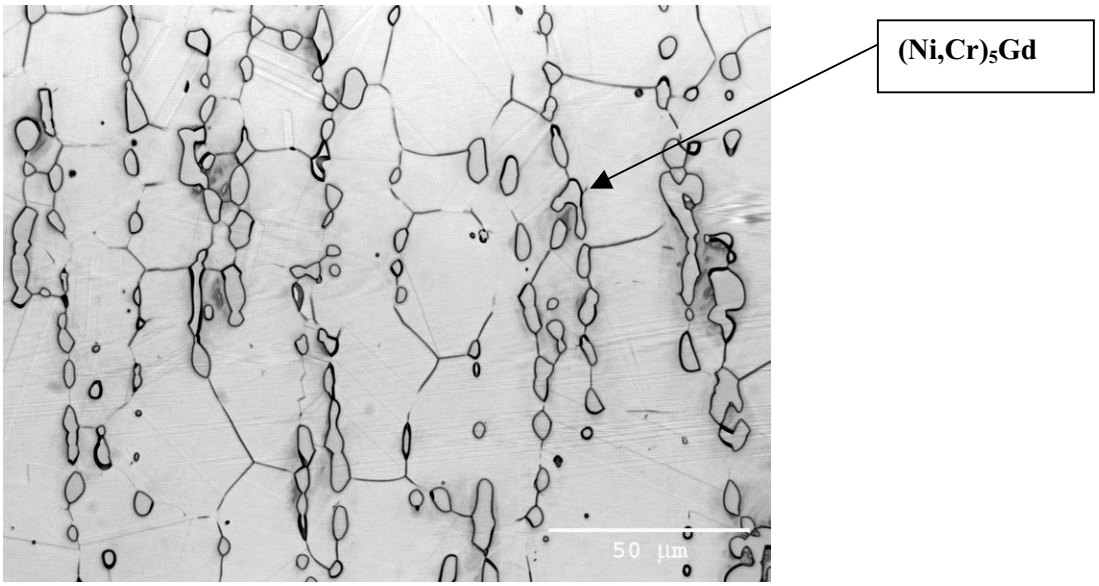

FIGURE 2 – LOM of Heat M322

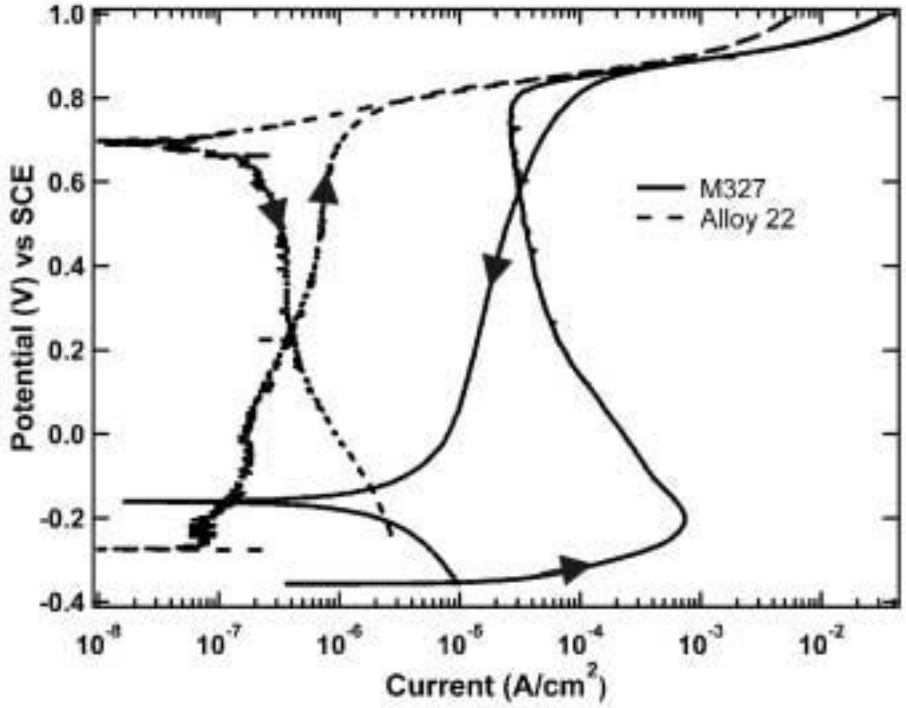

FIGURE 3 - CPP scans for M327 and Alloy 22 specimens obtained in 0.1 M HCl at 30°C

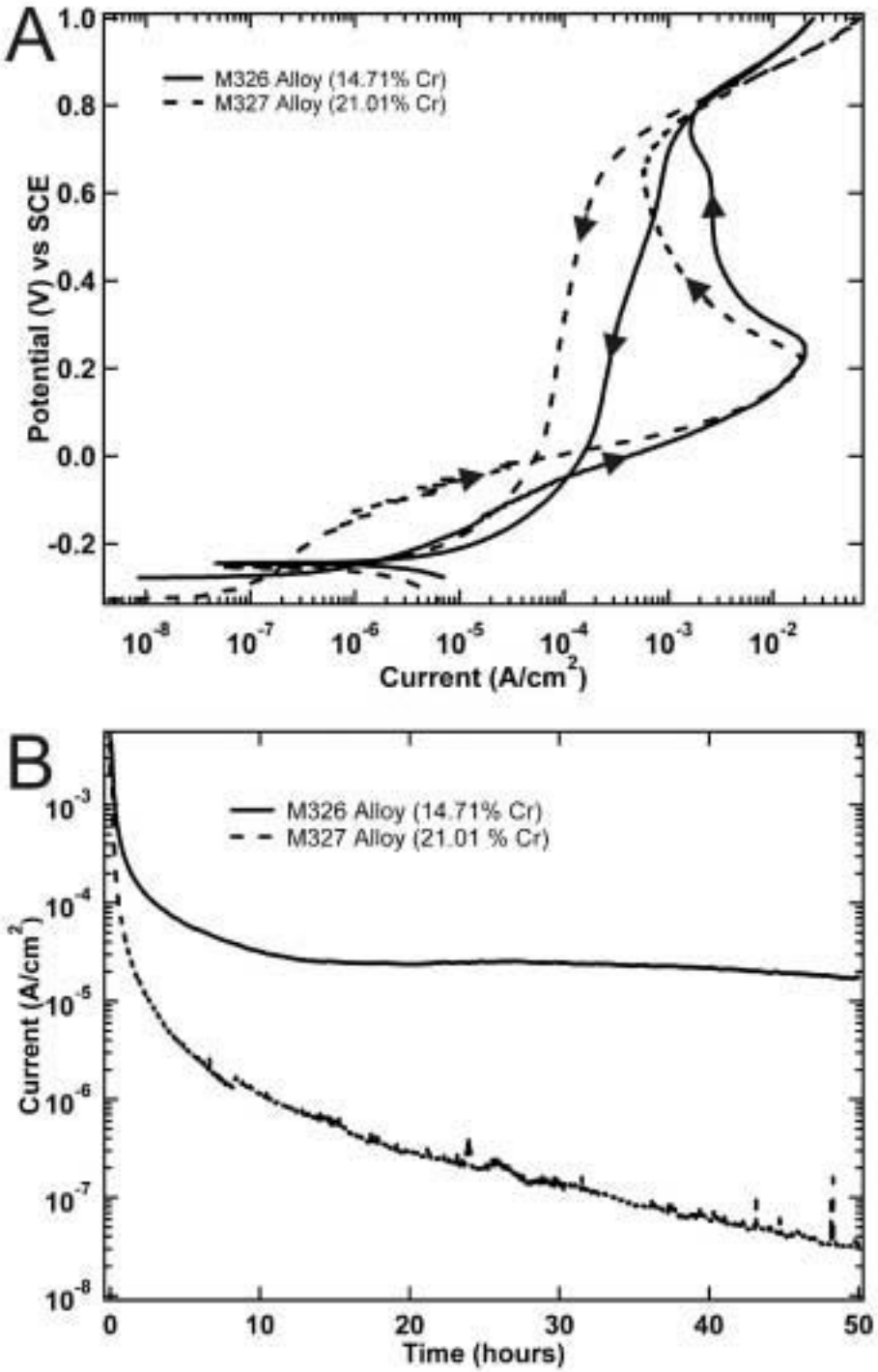

FIGURE 4 - Comparison of CPP (A) and PS (B) performance of alloys M326 and M327, 0.028 M NaCl, 30ºC, PS test run at +0.20V

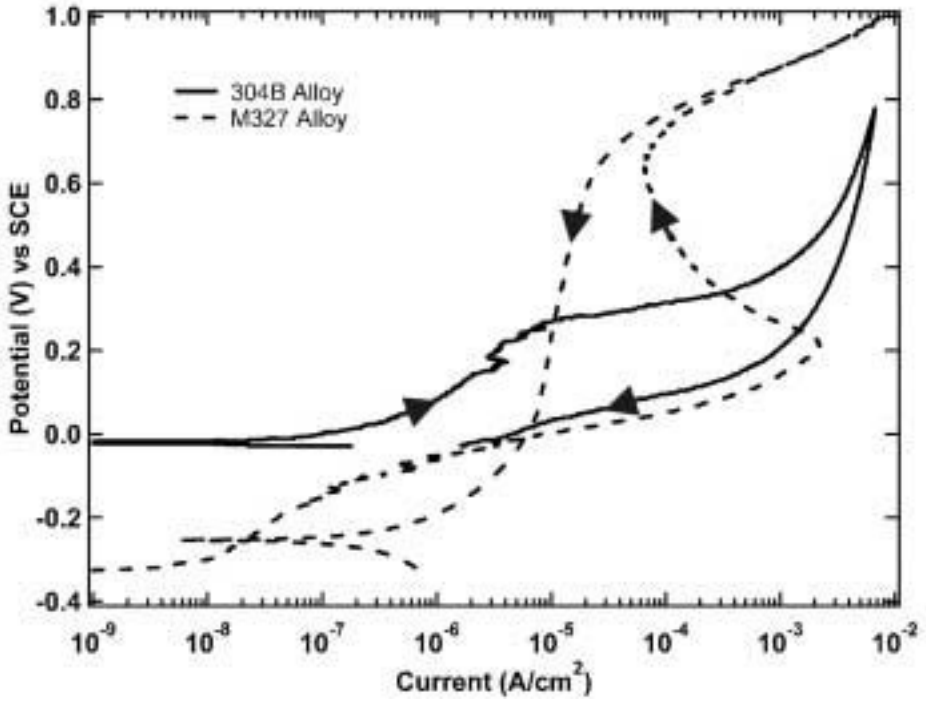

FIGURE 5 - CPP scans of 304B6 and M327 specimens in 0.028 M NaCl at 30°C. Note that the Reversal Potential was 0.8 V for 304B6

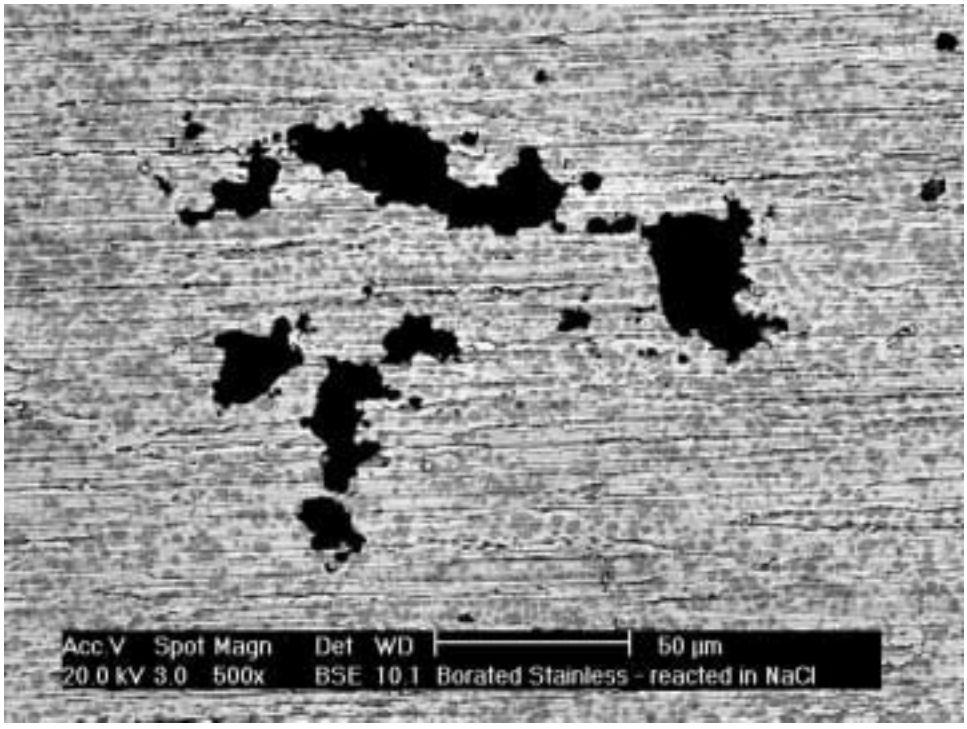

FIGURE 6 - SEM micrographs of 304B6 following two CPP scans, magnification 500X, same specimen as shown in Figure 5

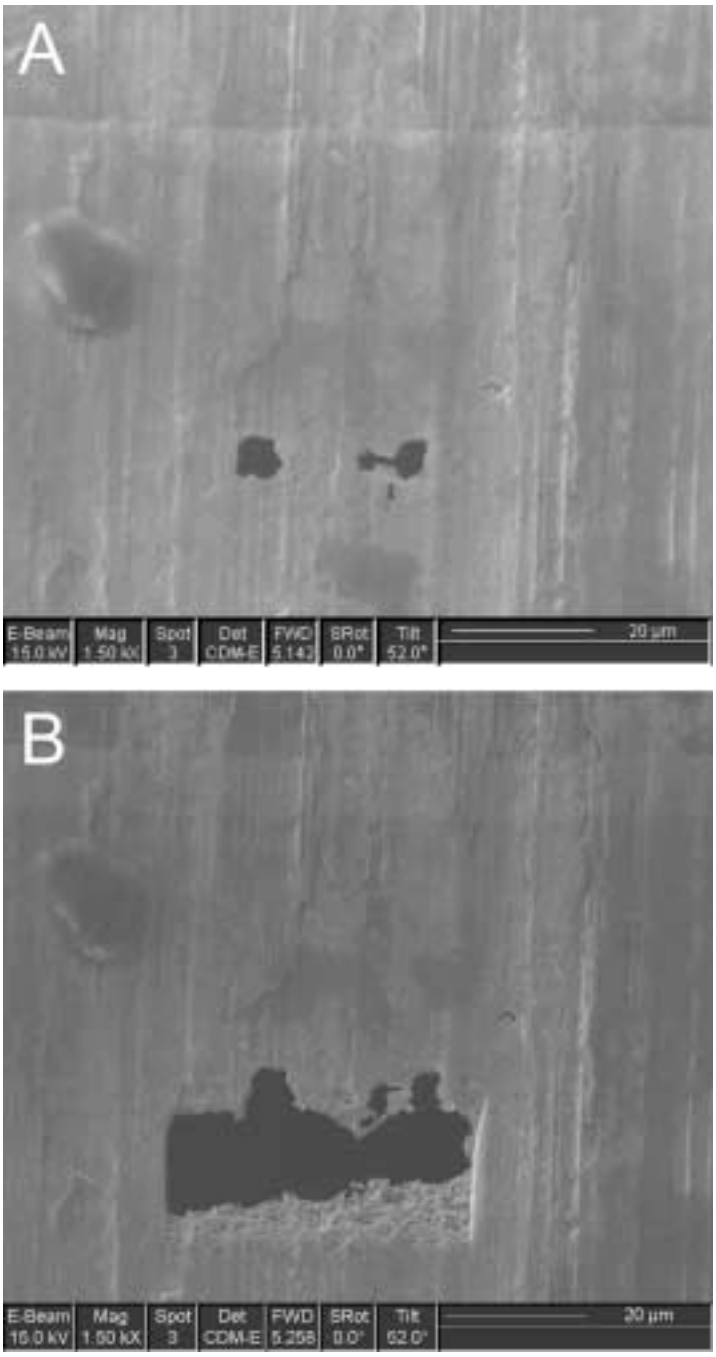

FIGURE 7 - SEM images (a) before and (b) after FIB sectioning of a 304B6 pit formed by potentiodynamic testing

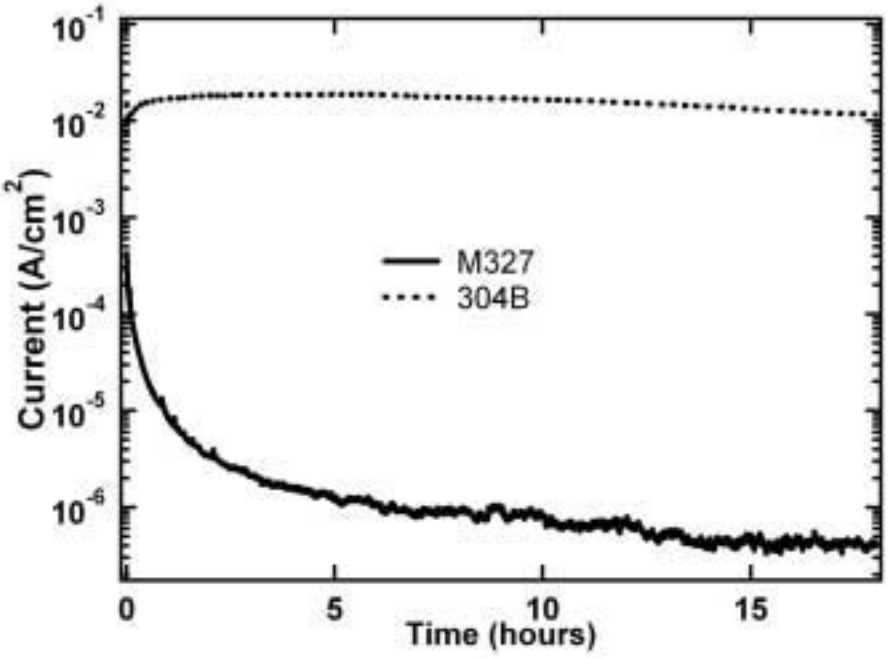

FIGURE 8 - PS curves for M327 and 304B6 specimens held at 0.20 V at 60°C in 0.1 M HCl

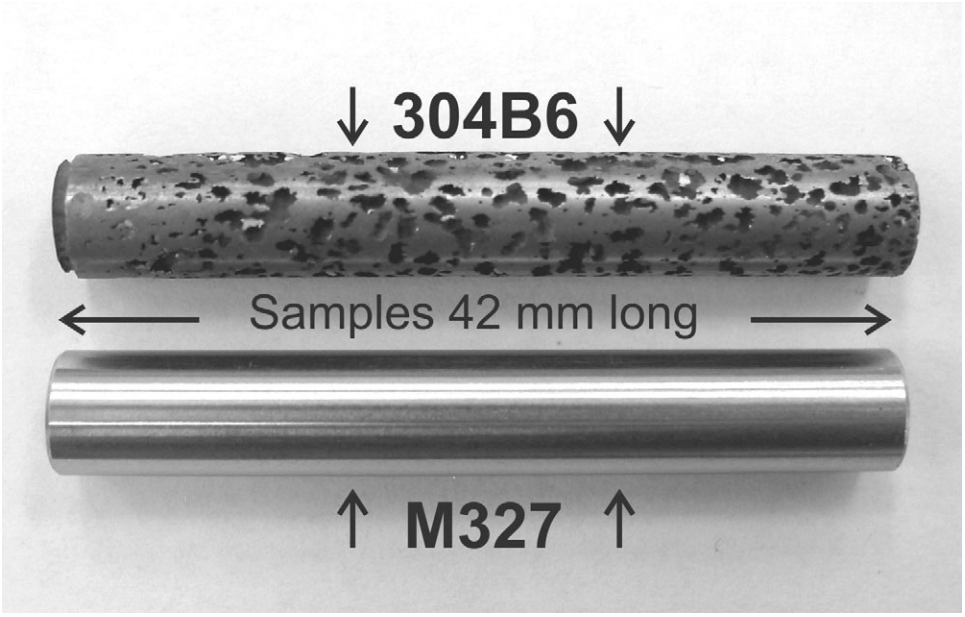

FIGURE 9 - Photographs of M327 and 304B6 specimens following PS test shown in Figure 5

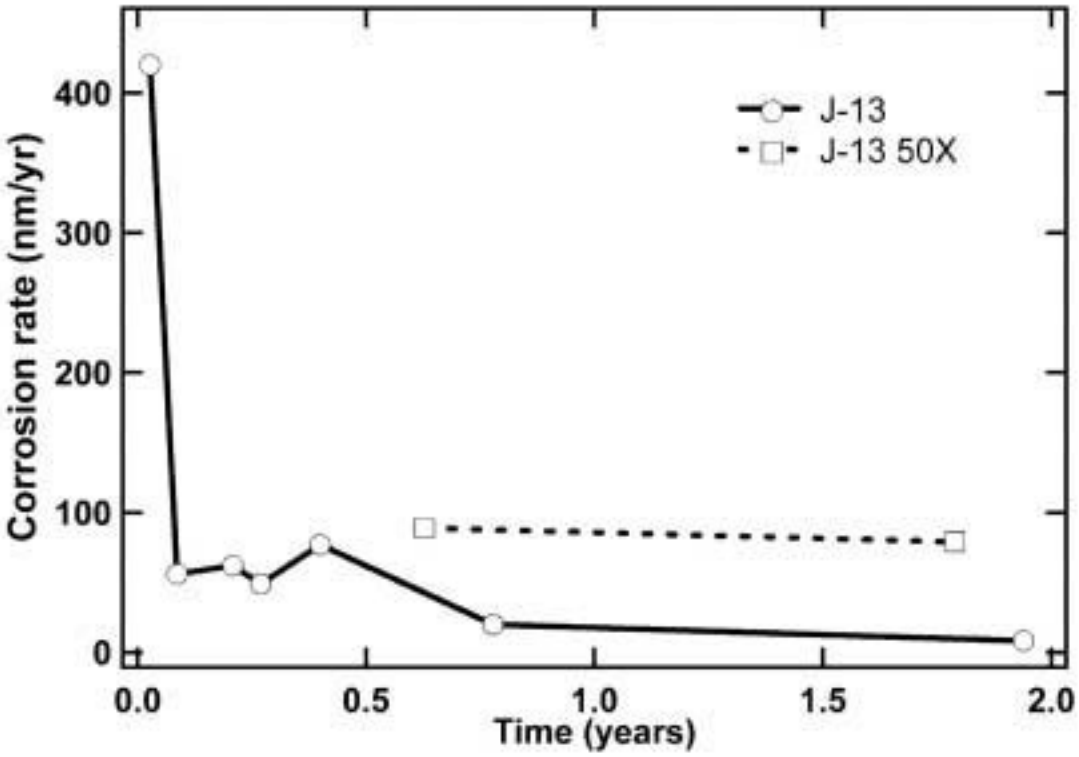

FIGURE 10 - The average corrosion rate for three M322 specimens immersed in J-13 and J-13 50X solutions at 30°C

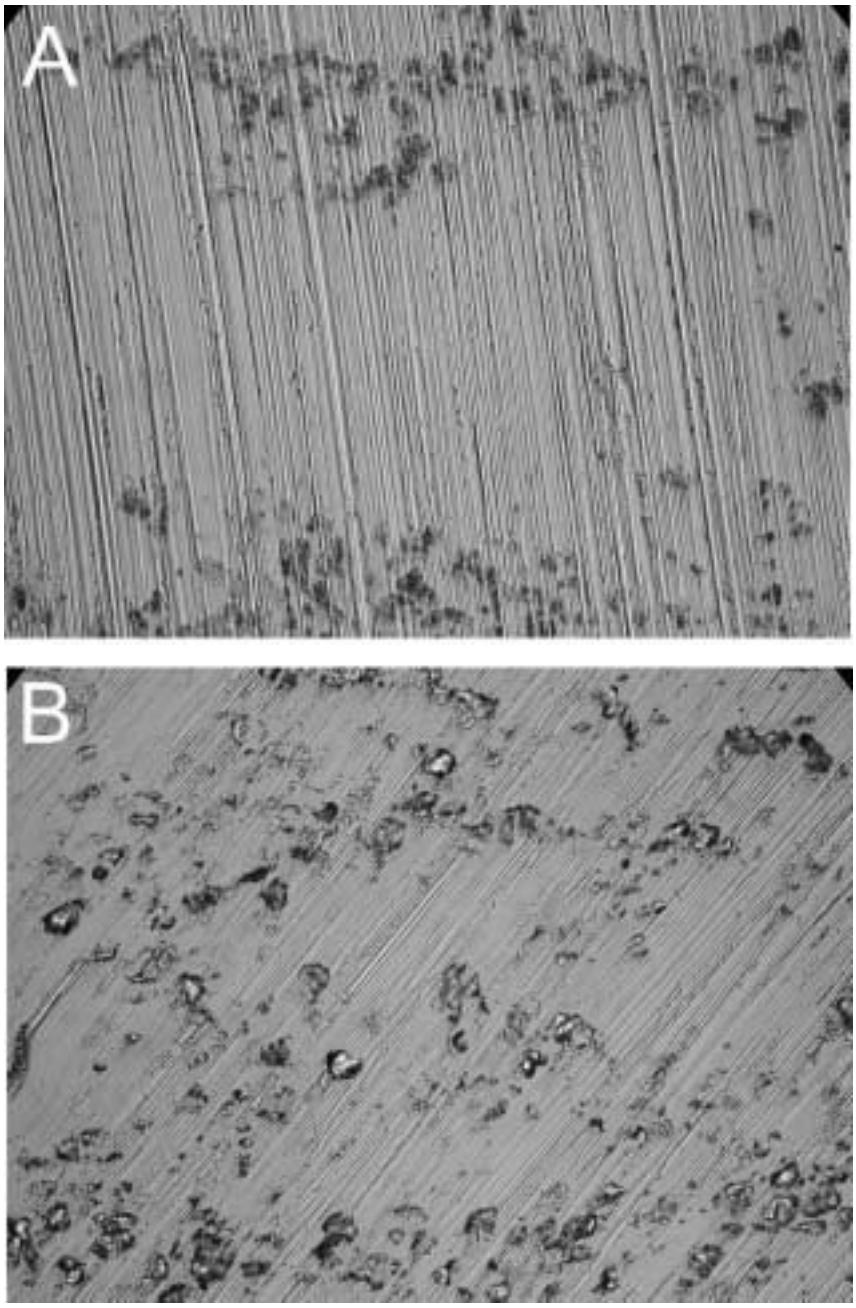

FIGURE 11 - LOM images taken at 500X magnification of M322 specimens exposed to A) J-13 and B) J-13 50X analyzed after the final data point taken in Figure 10

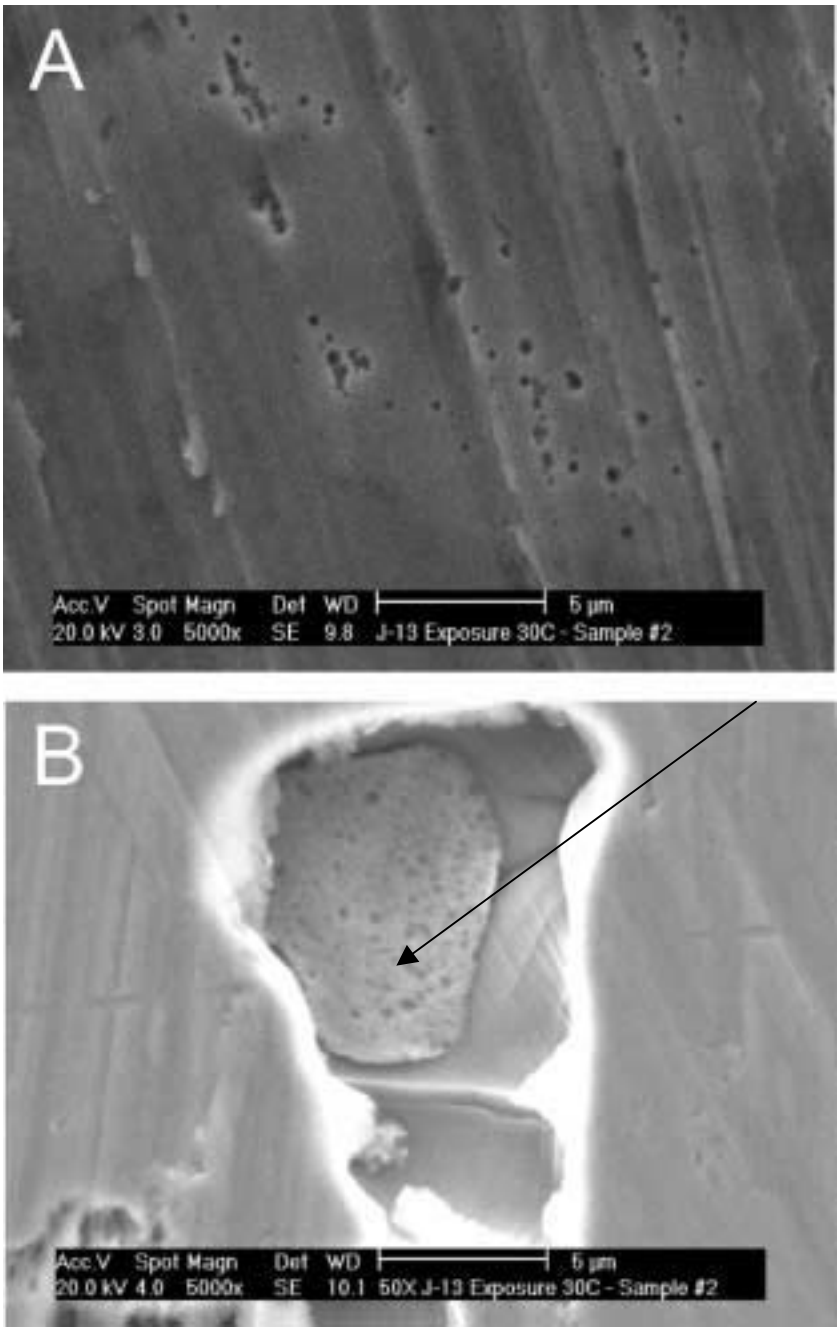

FIGURE 12 - SEM images taken at 5000X magnification of M322 specimens exposed to A) J-13 and B) J-13 50X analyzed after the final data point taken in Figure 10